Optical diagnosis of the progression and reversal of CCl_4 induced liver injury in rodent model using minimally invasive autofluorescence spectroscopy

Shaiju S. Nazeer [a], S Sandhyamani [b], Ramapurath S. Jayasree [a] *

[a]Biophotonics and Imaging Lab

Biomedical Technology Wing

Sree Chitra Tirunal Institute for Medical Sciences & Technology,

Poojappura, Thiruvananthapuram - 695 012,

Kerala, India.

[b]Department of Pathology

Sree Chitra Tirunal Institute for Medical Sciences & Technology,

Thiruvananthapuram - 695 011,

Kerala, India.

Correspondence to:

*Dr. R. S. Jayasree

Phone : +91 4712520273 (O) / 9495948221 (M), Fax:+91 471 2341814

Email – jayasree@sctimst.ac.in

Abstract

Liver cancer is the fifth most common cancer in men and seventh most common cancer in women worldwide. Intoxicant induced liver injury is one of the major causes for severe structural damage with fibrosis and functional derangement of the liver leading to cancer in its later stage. This report focuses on the minimally invasive autofluorescence spectroscopic (AFS) studies on intoxicant, carbon tetrachloride (CCl_4) induced liver damage in a rodent model. Different stages of liver damages including the reversed stage, on stoppage of intoxicant are examined. Emission from prominent fluorophores such as collagen, nicotinamide adenine dinucleotide (NADH), flavin adenine dinucleotide (FAD) and variations in redox ratio have been studied. A direct correlation between the severity of the disease and the level of collagen and redox-ratio was observed. On withdrawal of the intoxicant, a gradual reversal of the disease to the normal condition was observed as indicated by the decrease in collagen level and redox-ratio. Multivariate statistical technique, principal component analysis followed by linear discriminant analysis (PC-LDA) was used to develop diagnostic algorithms for distinguishing different stages of liver disease based on spectral features. The PC–LDA modeling on minimally invasive AFS dataset yielded diagnostic sensitivities of 93%, 87% and 87% and specificities of 90%, 98% and 98% respectively, for pair-wise classification between normal, fibrosis, cirrhosis and reversal conditions. We conclude that AFS along with PC–LDA algorithm has the potential for rapid and accurate minimally invasive diagnosis and detection of structural changes due to liver injury resulting from various intoxicants.

Keywords

Liver injury; intoxicant; collagen; redox ratio; minimally invasive evaluation; multivariate analysis

1. Introduction

Liver cancer is the sixth most frequently diagnosed cancer and the third most leading cause of cancer deaths worldwide. It is the second and sixth leading cause of cancer deaths among men and women respectively. Hepatocellular carcinoma (HCC) is the foremost histological subtype among primary liver cancers accounting for 70 to 85% of the total liver cancer incidence[1, 2]. Hepatitis C (HPC) virus infections are the prime cause for HCC. Excess intake of intoxicants also account for the disease progression. Synergetic interaction between HPC infections and intoxicants further increase the chance of HCC incidence[1, 3, 4].

Alcohol is the most important and common intoxicant that affects liver. Other than alcohol, natural chemicals in plants like alkaloids, fungal toxins and pesticides from contaminated food, and high fructose and sucrose containing soft drinks also cause structural damages to liver [3-5]. The commonly used anticancer and antibiotic drugs like Amiodarone, Aspirin , Methotrexate can also cause severe hepatotoxicity and chronic architectural damage to liver on prolonged use[6].

Liver associated with the accumulation of extra cellular matrix (ECM) proteins is the prime characteristics of most of the chronic liver diseases. Excess ECM proteins distort the hepatic architecture, forming fibrous scar and subsequent development of nodules of regenerating hepatocytes[7]. Fatty liver is the earliest stage of liver damage that develops through fibrosis and later progress to cirrhosis which consequently result in HCC in many cases[8, 9]. Liver fibrosis and cirrhosis, the stages which precede HCC are both reversible with proper and timely medical intervention [10]. This emphasises the need and importance of early diagnosis of the type and severity of hepatic damage when it is in a manageable stage.

Biopsy followed by histopathology is considered as the gold standard for screening liver fibrosis and cirrhosis associated with malignancy. However, the accuracy of this technique highly depends on tissue staining and morphological pattern recognition by an expert pathologist. Moreover, this technique is time consuming and has limited statistical confidence level due to inherent operator variability[11]. Therefore more sensitive screening methodologies are necessary to overcome the limited molecular detection capabilities of currently available immunohistochemical methods. *In vivo* and *ex vivo* modalities of optical techniques such as fluorescence, diffuse reflectance, Raman and infrared spectroscopy are able to differentiate molecular descriptors within tissue and are emerging diagnostic tools [11-22].

In this study, we demonstrate the potential of AFS as minimally invasive diagnostic tool to monitor biochemical changes within the liver tissue. Using this technique, we also demonstrate the functional reversal and regeneration capacity of liver after discontinuation of the intoxicants. We propose that the expected biochemical changes of collagen, NADH and FAD can be evaluated *in vivo* using optical spectroscopy during liver tissue transformations. For this, different stages of liver disease like fibrosis and cirrhosis on intoxicant, CCl_4 induced models were studied. A group of control animals and a group of animals that showed reversal of the diseased stage to normal condition, on stoppage of intoxicant has also been studied. A comparison of the results with histological evaluation was also carried out. The exact differentiation between different groups and validation of the dataset using the spectral data was done using PC-LDA.

2. Materials and methods

2.1. Animal model development

The animal model for liver damage was developed using a methodology described earlier[10, 23]. Institute Animal Ethics Committee of Sree Chithra Tirunnal Institute for Medical Sciences and Technology has approved the study (Order no: B 2982011 IX, dated: 19-10-2011). 20 male Wistar rats (~250 g) were used totally. Animals were grouped as control, fibrosis, cirrhosis and reversal with 5 animals in each group. Animals were treated twice a week, intraperitoneally, with equal parts (1:1) of CCl_4 and olive oil. A concentration of 0.2 ml/100 g of body weight of the mixture was injected for the first two weeks followed by a reduced concentration of 0.1 ml/100 g for the following weeks. Application of the mixture for 6 and 8 weeks confirmed development of fibrosis and cirrhosis respectively. Control animals were treated with identical volume of olive oil for 8 weeks. One group of animals with cirrhosis was followed up for 12 weeks without any further exposure to the intoxicant to study functional and morphological reversal of the liver damage. After 3 days of specified duration for the induction of fibrosis or cirrhosis, minimally invasive spectral acquisition was carried out. Prior to this, animals were anaesthetized using standard dosage of ketamine (70 mg/kg) and xylazine (5 mg/kg). A small incision was made on the ventral side of the anesthetized animal just outside the liver to facilitate *in vivo* spectral acquisition using the fiber optic probe.

2.2. Fluorescence spectroscopy instrumentation

Spectrofluorometer (Fluorolog-III; Jobin Yvon Inc., USA) with a fiber optic probe was used for minimally invasive autofluorescence measurements. The instrument consists of a 450 W Xenon arc lamp, photomultiplier tube as detector, a double excitation and a double emission monochromator. A bifurcated Y type fiber-optic probe coupled to the sample compartment facilitated *in vivo* measurements. This multimode fiber-optic probe with an outer diameter 1 cm consists of illumination fibers and collection fibers with numerical aperture of 0.22. One arm of the Y type fiber-optic probe is connected to the source. The desired excitation wavelength was selected and transmitted to the site through this arm. The Y-type fiber optic probe originating from the spectrometer merges to become a single fiber bundle at the distal end of the fiber which is in contact with the animal. The received fluorescence signal is directed back to the spectrometer through the other arm of Y type fiber-optic probe. The fiber probe is so designed that a central single excitation fiber having a diameter of few micrometers is surrounded by a bundle of emission fibers. The diameter of this collective fiber bundle is 0.5 cm and the total diameter along with the metallic cladding makes it thicker to 1 cm. Using Datamax™ software (Datamax, Round Rock, Texas, USA), excitation wavelength of 320 nm is selected and emission spectra in the range 350 to 550 nm with 1 nm increment were recorded from twelve different sites of the liver from all animals.

2.3. Data preprocessing and analysis

All spectra were baseline corrected and the data in 350 – 550 nm range were extracted. These spectra were normalized with respect to the intensity at 460 nm. On the normalized data, Gaussian curve fitting was done for precise analysis of peak position, intensity and bandwidth (full width at half-maximum) of 380 nm peak. Area under the curve and peak intensity for each group were extracted and subjected to one way analysis of variance (ANOVA) using the statistical software SPSS-17 (SPSS Inc., Chicago, Illinois).

2.4. Optical Redox ratio

The optical redox ratio was calculated on the basis of emissions from flurophores, NADH and FAD using the following equation:

$$\text{Optical redox ratio} = \frac{\text{FAD}_{\text{intensity}}}{\text{NADH}_{\text{intensity}} + \text{FAD}_{\text{intensity}}}$$

where FAD $_{\text{intensity}}$ and NADH $_{\text{intensity}}$ are the emission intensities at 520 and 460 nm, respectively[17, 24].

2.5. Multivariate analysis

Large dimensional spectral space (spectrum ranging from 350 to 550 nm with a data set of 200 intensities) often results in inefficiency in execution of conventional statistical analysis and clustering algorithms (e.g., soft independent modeling of class analogy, LDA etc.). PCA is the best method usually adopted to reduce these spectral data to smaller manageable components without losing the useful informations. PCA simplifies the complex multidimensional dataset and extract the key variables within the dataset as loadings and scores. These loading vectors and PC scores extracted are mutually related to the original spectrum. ANOVA was then used to identify the most significant PCs ($p < 0.05$) for differentiation between different liver tissue types. These PC scores are fed to the development of LDA algorithms for multiclass classification. LDA determines the discriminant function that maximizes the variances between groups while minimizing the variances between members of the same group[12].

Performance of the diagnostic algorithms provided by PC-LDA models to predict the tissue groups was estimated in an unbiased manner using leave-one tissue site-out, cross-validation method. This method of cross validation produces a confusion matrix that compares predicted versus actual group membership[25]. Using the algorithm provided by PC-LDA model, a training data set (50 spectra in each group) was created initially. As this algorithm is the predictor of group membership, we have performed blind-test using the remaining spectral data (10 spectra in each group) to further assess the suitability of the training data set. Binary calculations were done on these results based on PC-LDA scores on both training and blind test in order to obtain sensitivity and specificity of the diagnostic algorithm developed.

Performance level of the PC–LDA modeling for tissue classification is further assessed by receiver operating characteristic (ROC) curve method. ROC curves were generated by successively changing the thresholds to determine correct and incorrect classifications for all subjects [12].

2.6. Histological Evaluation

Animals were sacrificed immediately after spectral acquisition and liver biopsies were taken out from one animal of each group representing normal, fibrosis, cirrhosis and reversal of cirrhosis. The liver specimens were fixed in 10% buffered neutral formalin for 48 hrs. Tissue sections were processed through graded alcohol and embedded in paraffin. Histopathological analysis was carried out on 5 μ thick sections using Hematoxylin and Eosin (H&E), and Masson's trichrome (MT) staining methods to assess the parenchymal changes and the degree of fibrosis within the tissue.

3. Results

3.1. Fluorescence Spectral features

High quality AF spectra from liver tissue were acquired minimally invasively using 320 nm excitation wavelength. Fig. 1A shows the normalized and baseline corrected mean AF spectra ($n = 60$ in each group) of control, fibrosis, cirrhosis and reversal liver. Broad peaks were observed around 380 and 460 nm with a shoulder around 520 nm, in all the spectra. The emission peak around 380 nm is less intense for control liver and more intense for fibrosis and highly intense for cirrhosis compared with control liver. Interestingly, the intensity of this peak reduces from cirrhosis to reach the level of normal controls in the case of reversal liver. Area under fluorescence peak also shows a similar trend (Fig. 1B). Spectra from control liver showed a minimal area for this peak whereas fibrosis and cirrhosis showed successive increase and reversal showed a subsequent decrease. Pair wise ANOVA was performed on the peak intensity and area under the peak for the groups, control-fibrosis, fibrosis-cirrhosis and cirrhosis-reversal. Significant difference ($p < 0.005$) in peak intensity and area under the peak is observed for all pairs considered.

As we have normalized the whole spectra with respect to NADH emission peak at 460 nm, evaluation of peak intensity and area is not relevant here. Since normalization has no influence on the peak shift, the information regarding the same has been considered. For control liver, maximum intensity for this peak is observed at 463 nm, whereas for fibrosis and cirrhosis maximum intensity is observed at 459 and 457 nm respectively. In the case of reversed condition, this peak resumes back to 462 nm indicating its similarity to that of the normal controls. Considering the emission properties of NADH with respect to the three different conditions, a clear blue shift is observed for fibrosis from that of the control which becomes more prominent as it progresses to cirrhosis. This blue shift disappears in the case of reversed condition with an observed emission of 462 nm.

The emission peak around 520 nm is well defined in the case of cirrhosis, whereas it appears as a very weak shoulder in control, fibrosis and reversal. Variation in intensity of this peak follows the same pattern as that of 380 nm peak. Significant difference ($p < 0.005$) in the 520 nm peak intensity is also observed for control-fibrosis, fibrosis-cirrhosis and cirrhosis-reversal pairs.

3.2. Optical redox ratio

The Box-and-Whisker plot relating the variations in redox ratio of different groups is shown in Fig. 2. Drastic increase in redox ratio is observed for fibrosis and cirrhosis compared to normal controls with the increase being highly significant in the case of cirrhosis. Redox ratio has come down considerably for reversal and reaches a level similar to that of the normal control. Pair wise ANOVA between control-fibrosis, fibrosis-cirrhosis and cirrhosis-reversal shows significant difference ($p < 0.005$) in the redox ratio for all pairs considered.

3.3. Multivariate analysis

We have employed multivariate statistical tool PC-LDA to develop effective diagnostic algorithms for tissue classification based on AF spectra. Initially a training dataset of 50 spectra (10 spectra from each animal) from each group was used for this purpose. For the classification of different liver tissues types, the first seven principal components from each group were extracted. These extracted principal components contain ~99% of the total variance of diagnostically significant AF spectral features. These significant PC's are then fed into pair-wise discriminant analysis model to develop effective diagnostic algorithms for classification. The resultant pair-wise discriminant function scores are presented in Fig. 3A. A discrimination line drawn at 0 gives good differentiation results for all the pairs considered. Position of pairwise discrimination scores were utilized to obtain diagnostic accuracy results. Diagnostic accuracies such as sensitivity and specificity were evaluated using the true positive and negative, and false positive and negative values obtained from the position of these discriminant scores. Sensitivity of 94%, 86%, and 98% with corresponding specificities of 92%, 98% and 86% were obtained for pairs, control-fibrosis, fibrosis-cirrhosis and cirrhosis-reversal respectively in the discrimination (Table 1).

In order to validate the reliability of the training set, a blind-test was carried out in 10 spectra (2 spectra from each animal) from each group. Discriminant function scores from blind test were inserted into the scatter plot of the training set for validation (Fig. 3A). The developed algorithm could correctly classify eight spectra as control and nine spectra as fibrosis of control-fibrosis pair (with two control spectra misclassified as fibrosis and one fibrosis spectra misclassified as control), ten spectra as fibrosis and nine spectra as cirrhosis of fibrosis-cirrhosis pair (with one cirrhosis spectra misclassified as fibrosis), and nine spectra as cirrhosis and ten spectra as reversal in the cirrhosis-reversal pair (with one cirrhosis spectra misclassified as reversal). Classification results of blind test leads to sensitivity of 90%, 90% and 100% with specificity of 80%, 100% and 90% respectively for control-fibrosis, fibrosis-cirrhosis and cirrhosis-reversal pairs.

Further, to evaluate the performance of pairwise PC–LDA based diagnostic dataset for liver tissue classification, the integration areas under receiver operating characteristic (ROC) curves (Fig. 3B) were generated from the pairwise discriminant score by varying the discrimination threshold levels. The areas under the ROC curves are encouraging with values

0.983, 0.960, and 0.954 respectively for the pairs of control-fibrosis, fibrosis-cirrhosis and cirrhosis-reversal.

Apart from pair wise PC–LDA, the results were further represented in the form of confusion matrix considering all the four groups within a classification model (Fig. 4 and S1†). Clustering of resultant discriminant scores is observed with each class being mostly pooled with in coherent point clouds. Furthermore, majority of the discriminant scores of each group can be represented within an ellipse that corresponds to the classification model's confidence interval. Average of the discrimination score for each group is represented as centroids (star symbol). These group centroids are well separated and are clearly differentiable with considerable distance between each group. Interestingly, the position of centroid for the group reversal lies near to the discriminant score clusters of control and fibrosis. This LDA confusion matrix indicated 55 out of 60 control spectra as correctly classified, where 5 spectra were misclassified as fibrosis. For fibrosis, only 33 spectra out of 60 were correctly classified, while 4, 1 and 22 spectra were misclassified as control, cirrhosis and reversal respectively. In the case of cirrhosis, 52 spectra were correctly classified, whereas 1, 1 and 6 spectra were misclassified as control, cirrhosis and reversal. In the case of reversal, LDA yielded 42 correct classifications and 7, 10 and 1 spectra were misclassified as control, fibrosis and cirrhosis respectively. These results are summarized in Supplementary Table 1.

3.4. Histological evaluation

H&E and MT stained liver sections of control, fibrosis, cirrhosis and reversal animals are shown in Fig. 5. Compared with normal controls, H&E stained sections of fibrosed liver tissue showed increased inflammatory cell infiltration, ballooning of hepatocytes with infiltration of mononuclear cells, fatty changes and focal centrilobular necrosis. Compared to the fibrosis group, liver from cirrhosis group showed more parenchymal damage and fibrosis with some nodule formation. Interestingly liver sections of reversal group showed morphological pattern almost similar to that of normal control animals. MT staining revealed the variations in the degree of fibrosis between the groups. Fibrous tissue was seen as blue colored bands in the fibrosis group and as prominent wider bands surrounding nodules of liver cells in the cirrhosis group. In the reversal group, the liver morphology was almost similar to that in control animal with thin fibrous bands and less prominent nodules.

4. Discussion

In this study, we have investigated the minimally invasive AF spectral features of liver tissue from control animals, and those with CCl_4 induced fibrosis, cirrhosis and after reversal of cirrhosis by stoppage of the intoxicant. We have also utilized multivariate data analysis technique based algorithm to interpret the vast spectral information for exact discrimination of liver tissue having varying degree and type of damage. Spectral preprocessing techniques such as baseline correction and normalization were carried out to obtain better efficiency in the differentiation. Excitation wavelength of 320 nm was used to get emissions around 380, 460, and 520 nm respectively from the fluorophores collagen, NADH and FAD[17-21]. This excitation wavelength is most suitable for the characterization of tissue parameters based on these flurophores which are expected to have major changes during the liver abnormalities.

Excess synthesis and deposition of extra cellular matrix (ECM) proteins, predominantly collagen in liver is the prime reason for intoxicant induced liver damage[7, 26]. Therefore, quantitative analysis of collagen can provide clear idea about the degree of liver damage. Increase in the level of collagen observed in fibrosis stage and still higher level in the cirrhosis stage is attributed to the deposition of collagen in liver as a result of wound healing response and increased oxidative stress by intoxicants in liver cells[26, 27]. Decrease in the level of collagen on stoppage of intoxicants is due to ECM degradation and remodeling that takes place to regain the normal liver architecture and metabolism[23].

Oxidation of alcohol via alcohol dehydrogenase enzymes generates an excess of NADH in liver. This excess NADH promotes fatty acid synthesis and leads to liver damage[28]. The blue shifts observed for NADH emission peak around 460 nm for liver with fibrosis and cirrhosis can be attributed to the more immobilization of the same due to excess presence of this coenzyme[29]. Stoppage of intoxicant is expected to decrease the concentration of NADH. This decrease is reflected in the spectra of these animals where the emission of NADH resumes its original wavelength comparable to that of the normal animals.

NADH and FAD are the metabolic co-enzymes that act as electron donor and acceptor in the primary electron transport chain of the cellular metabolism. A relative change in this reduction and oxidation factor is termed as redox ratio. Variation in the cellular redox ratio is used to monitor the metabolic activity. Increase in the redox ratio is observed for fibrosis and cirrhosis compared to control liver. As redox ratio has an inverse correlation with the metabolic activity, this result implies the synergistic interaction between intoxicants and liver that reduces the metabolic activity. An exactly opposite version of this phenomenon is observed in cancer cells where increased cellular metabolic activity results in a decreased redox ratio[30]. Oxidative stress induced by intoxicants in liver could be the reason behind the elevation in redox ratio[31, 32].

Multivariate statistical analysis which incorporates the entire AF spectral data for analysis is more robust and precise way to differentiate between spectra having varying biochemical signatures. Initially, PCA was performed to reduce the high dimensional AF spectral dataset into a few important principal components. This reduced dataset was utilized as input for pairwise discriminant model. Fig. 3 A shows that the pairwise discriminant scores for different liver lesions form distinct, separate clusters. An overall sensitivity of 93%, 87% and 98% with corresponding specificities 90%, 98% and 87% were obtained for pairs, control-fibrosis, fibrosis-cirrhosis and cirrhosis-reversal respectively in discriminating the tissue, using the pairwise discriminant scores (Table 1). The ROC curves (Fig. 3B) of pairwise PC–LDA modeling further verifies the diagnostic efficiency of AF spectroscopy integrated with PC–LDA algorithm. An area under the ROC curve greater than 0.60 in discrimination is considered as a good classification model[33-35].

The discrimination results were further presented in the form of confusion matrix for more authenticity (Fig. 4 and S1†). Clustering of discriminant scores is observed for different groups. Mean of these scores were represented as centroids and the distance between centroids correspond to the difference in dimension between each group. This classification has been done based on the Mahalanobis distance. Mahalanobis distance is the multivariate measure of the separation of a point from the mean of a dataset in n-dimensional space. The sample has been assigned to the group from which it has shorter Mahalanobis distance[15]. Possibility of further discrimination between the clusters of each group was attempted by plotting ellipsoids obtained using the model confidence intervals for each class[36]. For control, fibrosis and reversal groups, the resultant ellipsoids were found to be small in size and the data points are clearly clustered. But for cirrhosis, the size of this ellipsoid is large and the data points are scattered compared to other three groups. This may be due to the spectral variation resulted due to the variation in the level of collagen. Excess level of collagen compared to its average is observed in nearly fifteen sites of cirrhosis liver which ultimately resulted in the scattering of the data points in the confusion matrix analysis. Interestingly, the position of the reversal group in this plot lies closer to fibrosis and control, and far away from cirrhosis. This clearly indicates the self regenerating ability of liver on stoppage of chronic intoxication after cirrhosis. This result gives an indication that AFS is a potential minimally invasive tool to diagnose liver diseases *in vivo* and this technique could be used for the early diagnosis of alcoholic liver disease and fatty liver disease of humans.

5. Conclusions

Minimally invasive autofluorescence spectroscopic analysis of liver diseases viz. fibrosis and cirrhosis, and a reversed stage of the condition have been reported for the first time. Multivariate analysis technique, PC-LDA on AF spectral data was successful in differentiating between different types and grades of liver lesions with high diagnostic sensitivity and specificity. Changes in flurophores like collagen, NADH and FAD were assessed using AF spectroscopy. These biomarkers have an essential role in structural and biochemical damage of liver due to chronic intoxication. Variation in metabolic activity and oxidative stress within liver was also analyzed using optical redox ratio. Therefore, AF spectroscopy holds great promise in minimally invasive *in vivo* diagnosis of early changes of fibrosis and cirrhosis that are usually associated with liver malignancy. AF spectral evaluation on higher degree of liver injury would help to get a better understanding of the intoxicant induced biochemical/structural changes in liver. The main limitation of this study is the practical difficulties encountered during the minimally invasive measurements due to the large size of the optical probe. We are in the process of development of an endoscope assisted minimally invasive laser induced, portable AF spectroscopy systems with smaller probe diameter which could solve this issue. Moreover, we are working on animal trials in larger sample size and we expect that this methodology could be used for clinical evaluation, in the near future.

Acknowledgments

The financial support received from the Board of Research in Nuclear Sciences, Department of Atomic Energy, Government of India is sincerely acknowledged. The authors acknowledge the support of Dr Sachin J Shenoy, Scientist, Division of *In Vivo* Models and Testing, SCTIMST for the support provided during minimally invasive spectral acquisition. Shaiju S. Nazeer acknowledges Council of Scientific and Industrial Research, India for the Senior Research Fellowship.

References

1. A. Jemal, F. Bray, M. M. Center, J. Ferlay, E. Ward and D. Forman, *CA Cancer J Clin*, 2011, 61, 69-90.
2. A. Jemal, M. M. Center, C. DeSantis and E. M. Ward, *Cancer Epidemiol Biomarkers Prev*, 2010, 19, 1893-1907.
3. H. O. Adami, A. W. Hsing, J. K. McLaughlin, D. Trichopoulos, D. Hacker, A. Ekbom and I. Persson, *Int J Cancer*, 1992, 51, 898-902.
4. F. X. Bosch, J. Ribes and J. Borras, *Seminars in Liver Disease*, 1999, 19, 271-285.
5. W. Nseir, F. Nassar and N. Assy, *World J Gastroenterol*, 2010, 16, 2579-2588.
6. L. A. Adams and P. Angulo, *Postgrad Med J*, 2006, 82, 315-322.
7. R. Bataller and D. A. Brenner, *J Clin Invest*, 2005, 115, 209-218.
8. G. C. Farrell and C. Z. Larter, *Hepatology*, 2006, 43, S99-S112.
9. J. K. Reddy and M. S. Rao, *Am J Physiol Gastrointest Liver Physiol*, 2006, 290, G852-858.
10. C. Constandinou, N. Henderson and J. P. Iredale, *Methods Mol Med*, 2005, 117, 237-250.
11. D. C. Fernandez, R. Bhargava, S. M. Hewitt and I. W. Levin, *Nat Biotechnol*, 2005, 23, 469-474.
12. M. S. Bergholt, W. Zheng, K. Lin, K. Y. Ho, M. Teh, K. G. Yeoh, J. B. So and Z. Huang, *Biosens Bioelectron*, 2011, 26, 4104-4110.
13. S. Feng, R. Chen, J. Lin, J. Pan, G. Chen, Y. Li, M. Cheng, Z. Huang, J. Chen and H. Zeng, *Biosens Bioelectron*, 2010, 25, 2414-2419.

14. S. Feng, R. Chen, J. Lin, J. Pan, Y. Wu, Y. Li, J. Chen and H. Zeng, *Biosens Bioelectron*, 2011, 26, 3167-3174.

15. J. L. Jayanthi, R. J. Mallia, S. T. Shiny, K. V. Baiju, A. Mathews, R. Kumar, P. Sebastian, J. Madhavan, G. N. Aparna and N. Subhash, *Lasers Surg Med*, 2009, 41, 345-352.

16. J. L. Jayanthi, N. Subhash, M. Stephen, E. K. Philip and V. T. Beena, *J Biophotonics*, 2011, 4, 696-706.

17. S. S. Nazeer, R. Asish, C. Venugopal, B. Anita, A. K. Gupta and R. S. Jayasree, *J Biomed Opt*, 2014, 19, 057013-057013.

18. S. S. Nazeer, A. Saraswathy, A. K. Gupta and R. S. Jayasree, *J Biomed Opt*, 2013, 18.

19. S. S. Nazeer, A. Saraswathy, A. K. Gupta and R. S. Jayasree, *Laser Phys*, 2014, 24.

20. A. Saraswathy, R. S. Jayasree, K. V. Baiju, A. K. Gupta and V. P. M. Pillai, *Photomedicine and Laser Surgery*, 2009, 27, 425-433.

21. S. N. Shaiju, S. Ariya, R. Asish, P. S. Haris, B. Anita, G. A. Kumar and R. S. Jayasree, *J Biomed Opt*, 2011, 16.

22. P. Venkatachalam, L. L. Rao, N. K. Kumar, A. Jose and S. S. Nazeer, *AIP Conference Proceedings*, 2008, 1075, 144-148.

23. J. P. Iredale, *J Clin Invest*, 2007, 117, 539-548.

24. N. D. Kirkpatrick, C. Zou, M. A. Brewer, W. R. Brands, R. A. Drezek and U. Utzinger, *Photochem Photobiol*, 2005, 81, 125-134.

25. A. Sahu, K. Dalal, S. Naglot, P. Aggarwal and C. M. Krishna, *PLoS One*, 2013, 8.

26. K. J. Thompson, I. H. McKillop and L. W. Schrum, *World J Gastroenterol*, 2011, 17, 2473-2481.

27. K. L. Yang, K. C. Hung, W. T. Chang and E. I. Li, *Comp Hepatol*, 2007, 6, 9.

28. C. S. Lieber, *Clin Chim Acta*, 1997, 257, 59-84.

29. A. A. Heikal, *Biomark Med*, 2010, 4, 241-263.

30. M. C. Skala, K. M. Riching, A. Gendron-Fitzpatrick, J. Eickhoff, K. W. Eliceiri, J. G. White and N. Ramanujam, *Proc Natl Acad Sci U S A*, 2007, 104, 19494-19499.

31. C. Bolukbas, F. F. Bolukbas, M. Horoz, M. Aslan, H. Celik and O. Erel, *Bmc Infect Dis*, 2005, 5.

32. D. P. Jones, *Rejuvenation Res*, 2006, 9, 169-181.

33. K. A. Smitha, A. K. Gupta and R. S. Jayasree, *Eur J Radiol*, 2013, 82, 857-861.

34. M. Gohulkumar, S. S. Nazeer, R.S. Jayasree, K. Gurushankar, N. Krishnakumar, *Anal Methods*, 2014, 6, 9744- 9753.

35. K. Gurushankar, S. S. Nazeer, M. Gohulkumar, R.S. Jayasree, R. M. Nirmal, N. Krishnakumar, *RSC Adv,* 2014, 4, 46896- 46906.

36. S. Stockel, S. Meisel, M. Elschner, P. Rosch, J. Popp, *Angew. Chem. Int. Ed.*, 2012, 51, 5339 –5342

Figure Captions

Graphical abstract. Schematic representation of the degree of intoxicant induced liver injury and regeneration and the minimally invasive analysis using autofluorescence spectral features.

Fig. 1. (A) Average fluorescence emission spectra of various degree of intoxicant induced liver injury (B) Area under the emission peak of collagen around 380 nm evaluated by Gaussian curve fitting. Data are shown as Mean $\pm$ SD.

Fig. 2. Variation in optical redox ratio for different grades of liver injury represented as Box-and-Whisker plot. The middle line represents the median. The bottom of the box is the 25th percentile and the top is the 75th. The line extending from the top of the box represents the upper extreme and the line extending from the bottom of the box represents the lower extreme.

Fig. 3. (A) Pairwise discriminant plot based on PC-LDA for different pairs of liver lesions. Solid symbols represent the results of training data set and the open symbols represent the validation data set. (B) The receiver operating characteristic curves of the discrimination using PC–LDA.

Fig. 4. PC-LDA score plots obtained using confusion matrix analysis. The ellipsoids display the model confidence intervals for each class.

Fig. 5. (A-D) Hematoxylin and eosin and (E-H) Masson's trichrome stained liver sections. Liver sections from (A, E) control, (B, F) fibrosis, (C, G) cirrhosis and (D, H) reversal group of animals showing variation in tissue architecture in the test group, with ballooning of hepatocytes, fatty change, fibrosis and nodule formation that are more prominent in cirrhosis animal than fibrosis animal. Liver from reversal animal appears similar to the control liver.

Table 1. Overall diagnostic accuracies obtained using multivariate analysis, PC-LDA for different lesion pairs consisting of 50 spectra in each group in the training set and 10 spectra in each group in the validation set.

Lesion pairs	Control versus Fibrosis		Fibrosis versus Cirrhosis		Cirrhosis versus Reversal	
	Sensitivity (%)	Specificity (%)	Sensitivity (%)	Specificity (%)	Sensitivity (%)	Specificity (%)
Training set	94	92	86	98	98	86
Validation set	90	80	90	100	100	90
Overall	93.33	90	86.67	98.33	98.33	86.67

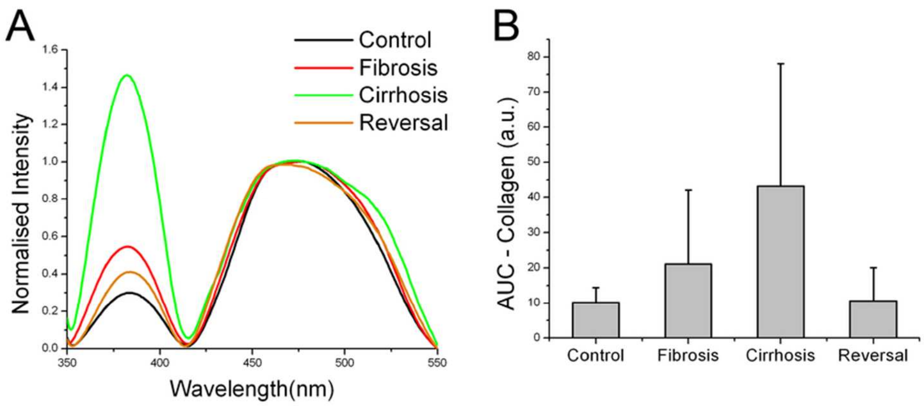

Fig. 1. (A) Average fluorescence emission spectra of various degree of intoxicant induced liver injury (B) Area under the emission peak of collagen around 380 nm evaluated by Gaussian curve fitting. Data are shown as Mean + SD.
80x33mm (300 x 300 DPI)

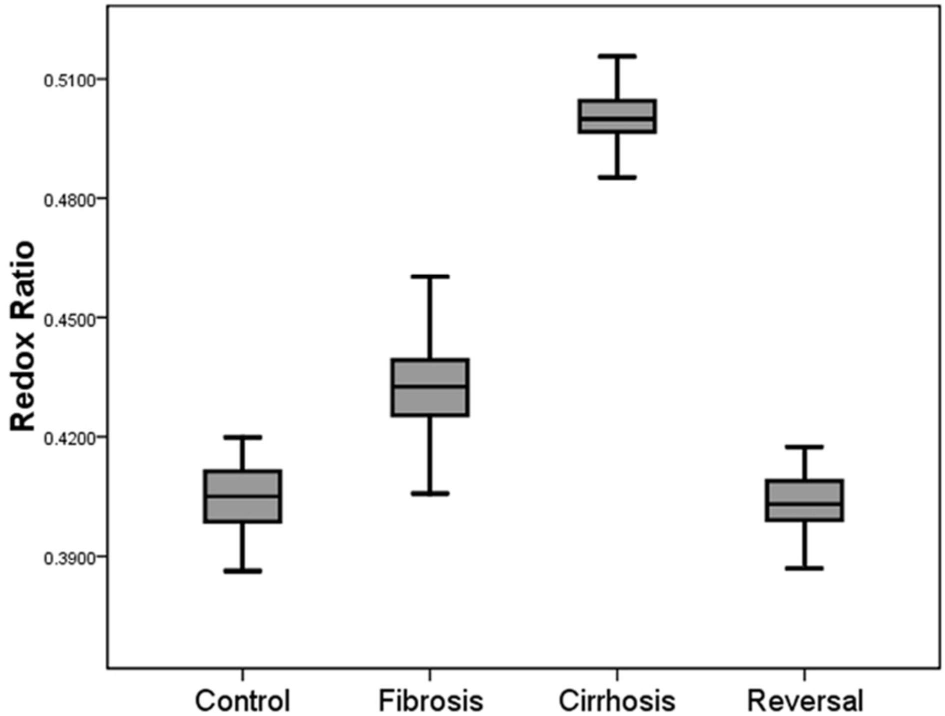

Fig. 2. Variation in optical redox ratio for different grades of liver injury represented as Box-and-Whisker plot. The middle line represents the median. The bottom of the box is the 25th percentile and the top is the 75th. The line extending from the top of the box represents the upper extreme and the line extending from the bottom of the box represents the lower extreme.
60x46mm (300 x 300 DPI)

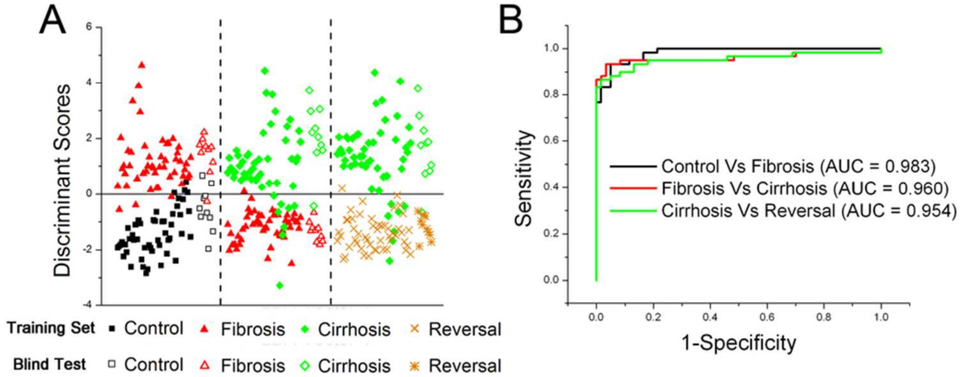

Fig. 3. (A) Pairwise discriminant plot based on PC-LDA for different pairs of liver lesions. Solid symbols represent the results of training data set and the open symbols represent the validation data set. (B) The receiver operating characteristic curves of the discrimination using PC–LDA.
84x34mm (300 x 300 DPI)

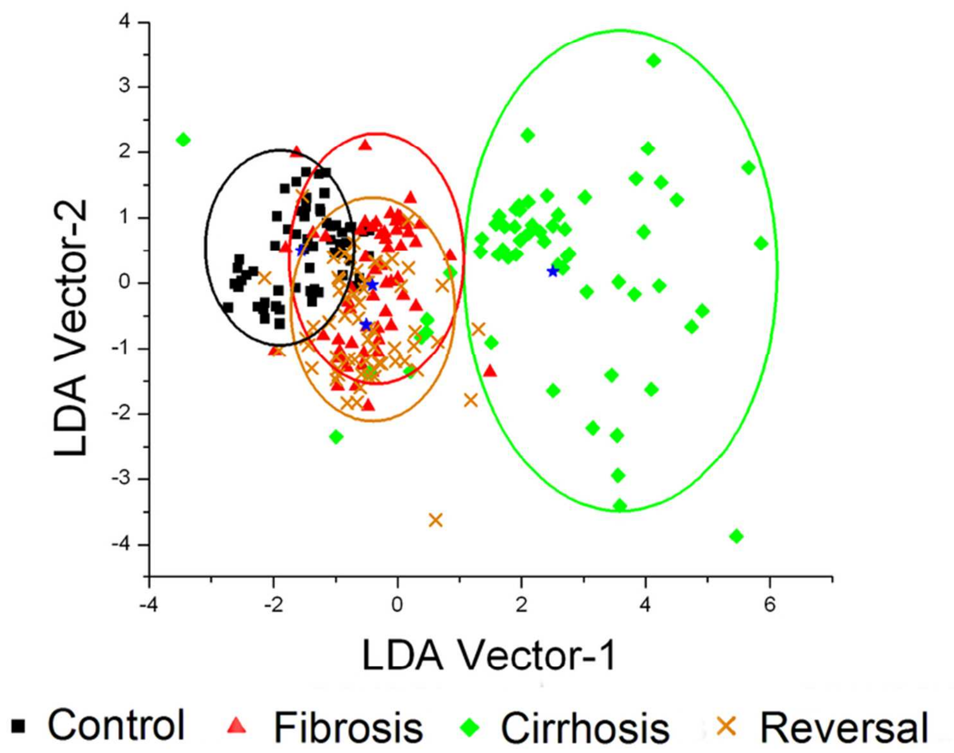

Fig. 4. PC-LDA score plots obtained using confusion matrix analysis. The ellipsoids display the model confidence intervals for each class.
69x57mm (300 x 300 DPI)

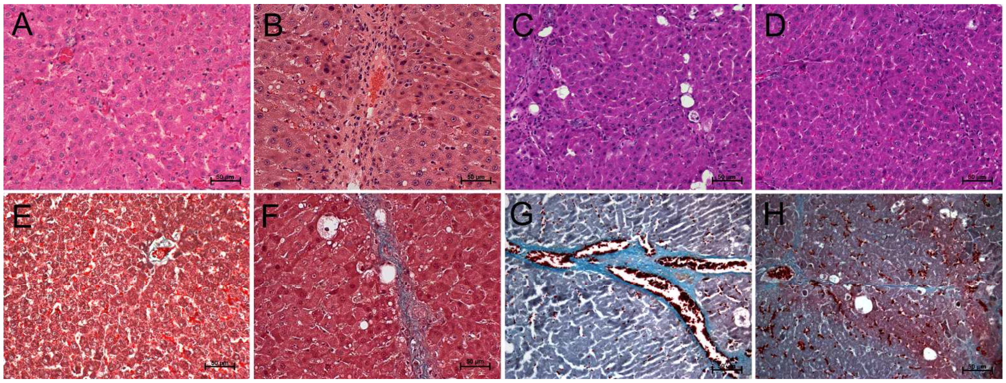

Fig. 5. (A-D) Hematoxylin and eosin and (E-H) Masson's trichrome stained liver sections. Liver sections from (A, E) control, (B, F) fibrosis, (C, G) cirrhosis and (D, H) reversal group of animals showing variation in tissue architecture in the test group, with ballooning of hepatocytes, fatty change, fibrosis and nodule formation that are more prominent in cirrhosis animal than fibrosis animal. Liver from reversal animal appears similar to the control liver.
265x99mm (300 x 300 DPI)